

Heterogeneous Hydroxyl-Directed Hydrogenation: Control of Diastereoselectivity through Bimetallic Surface Composition

Alexander J. Shumski, William A. Swann, Nicole J. Escorcía, and Christina W. Li*

Cite This: *ACS Catal.* 2021, 11, 6128–6134

Read Online

ACCESS |



Metrics & More



Article Recommendations



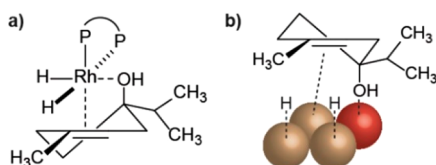
Supporting Information

ABSTRACT: Directed hydrogenation, in which product selectivity is dictated by the binding of an ancillary directing group on the substrate to the catalyst, is typically catalyzed by homogeneous Rh and Ir complexes. No heterogeneous catalyst has been able to achieve equivalently high directivity due to a lack of control over substrate binding orientation at the catalyst surface. In this work, we demonstrate that Pd–Cu bimetallic nanoparticles with both Pd and Cu atoms distributed across the surface are capable of high conversion and diastereoselectivity in the hydroxyl-directed hydrogenation reaction of terpinen-4-ol. We postulate that the OH directing group adsorbs to the more oxophilic Cu atom while the olefin and hydrogen bind to adjacent Pd atoms, thus enabling selective delivery of hydrogen to the olefin from the same face as the directing group with a 16:1 diastereomeric ratio.

KEYWORDS: directed hydrogenation, substrate direction, bimetallic nanoparticle, alloy, ensemble geometry

Substrate-directed hydrogenations are an important class of selective organic reactions that provide access to highly functionalized and diastereomerically pure products.^{1–4} High selectivity toward directed hydrogenation has been demonstrated using molecular catalysts based on Ir, Rh, and Co, in which the organometallic complex simultaneously activates and coordinates H₂, the directing group, and the alkene in a well-defined orientation at a single metal center in order to achieve facially selective addition of H₂ across the olefin (Scheme 1a).^{5–9} Heterogeneous systems based on supported metal

Scheme 1. Homogeneous vs Heterogeneous Directed Hydrogenation



nanoparticles tend to be more reactive, robust, and recyclable as hydrogenation catalysts than their molecular counterparts, but none have shown significant directing capability.^{10–12} A few examples using monometallic heterogeneous catalysts such as Raney Ni and supported Pd, Pt, and Rh nanoparticles have shown a mild directing group effect with alcohol, ether, and amine functionality, but the strength of the interaction between the directing group and the surface is weak compared to homogeneous complexes, resulting in poor diastereoselectivity.^{13–20}

In this work, we show that a bimetallic Pd surface is capable of achieving diastereoselective OH-directed hydrogenation when both metal atoms are available at the catalyst surface. We postulate that adsorption of the alcohol directing group to the more oxophilic alloying metal and activation of the alkene and hydrogen at adjacent Pd atoms result in diastereoselective delivery of hydrogen on the same face as the directing group (Scheme 1b). Previous work has shown that alloying pure Pd increases its selectivity for a variety of hydrogenation and condensation reactions, but these examples use the second metal primarily to temper the reactivity of the Pd surface in order to achieve semihydrogenation of alkynes and dienes or to alter chemoselectivity between multiple reaction pathways.^{21–36}

We began by synthesizing supported Pd–M (3:1) alloy nanoparticles through coimpregnation of metal precursor salts on Al₂O₃ followed by high temperature reduction at 800 °C in 5% H₂/N₂ to form the alloy. These Pd₃M/Al₂O₃ catalysts were screened in the hydrogenation of a model substrate, terpinen-4-ol, in cyclohexane under balloon pressure of H₂ at room temperature (Table 1). Well-ordered bimetallic surfaces with directing capability are expected to favor product P1, while no significant steric preference for P2 is expected in the absence of a directing effect.

Received: March 29, 2021

Revised: May 3, 2021

Published: May 6, 2021

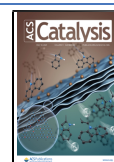
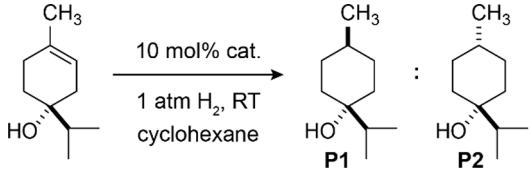


Table 1. Screening of Supported Pd-M Catalysts^a


Entry	Catalyst	Time	Conversion ^b	dr (P1:P2) ^b
1	Pd/Al ₂ O ₃	2 h	99%	1:1
2	Pd ₃ Fe/Al ₂ O ₃	2 h	99%	2:1
3	Pd ₃ Co/Al ₂ O ₃	2 h	99%	2:1
4	Pd ₃ Ni/Al ₂ O ₃	2 h	99%	3:1
5	Pd ₃ Cu/Al ₂ O ₃	2 h	43%	5:1
6	Pd ₃ Zn/Al ₂ O ₃	2 h	56%	4:1

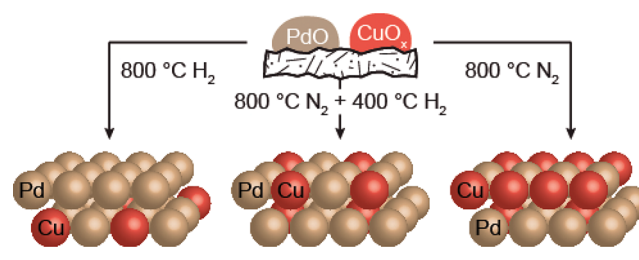
Pd ₃ Cu/SiO ₂				
7	RT H ₂	20 h	99%	1:1
8	600H ₂	20 h	95%	2:1
9	800H ₂	20 h	99%	3:1
10	600N ₂	20 h	98%	3:1
11	700N ₂	20 h	66%	10:1
12	800N ₂	20 h	30%	17:1
13	600N ₂ -400H ₂	20 h	99%	3:1
14	700N ₂ -400H ₂	20 h	95%	8:1
15	800N ₂ -400H ₂	20 h	99%	16:1
16	800N ₂ -800H ₂	20 h	99%	6:1

^a0.1 mmol substrate, 50 mg 2 wt % Pd-M catalyst, 5 mL cyclohexane, H₂ balloon ^bSingle run conversions and diastereomeric ratios (dr) determined by GC with decane as an internal standard.

Using a pure Pd/Al₂O₃ catalyst, we observe complete conversion of the substrate after 2 h and a diastereomeric ratio for P1/P2 (dr) of 1:1, revealing that pure Pd nanoparticles are incapable of binding the hydroxyl directing group, in line with previous reports on Pd/C catalysts (Table 1, entry 1).⁵ Pd₃Fe, Pd₃Co, and Pd₃Ni catalysts show conversions similar to pure Pd with slight increases in dr to 2–3:1 toward the directed product (Table 1, entries 2–4). However, incomplete alloying and phase segregation of the two metals is observed, which results in low directivity (Figure S1).³⁷ The late transition metal alloys Pd₃Cu and Pd₃Zn show suppressed conversion and elevated diastereoselectivity relative to monometallic Pd, suggesting that a larger proportion of the catalyst forms the bimetallic structure (Table 1, entries 5 and 6). In this initial screen, Pd₃Cu showed the highest diastereoselectivity for the directed hydrogenation with a 5:1 dr at 43% conversion in 2 h. A control sample containing only Cu showed no conversion under these conditions (Table S12, Figure S26).

Pd–Cu alloys are known to show dynamic surface reconstruction during thermal annealing depending on the gas atmosphere and temperature regime.^{38–40} Pd atoms preferentially migrate to the surface in the presence of strongly adsorbing gases such as H₂ and CO while Cu segregates to the surface under high-temperature inert gas or vacuum conditions (Scheme 2).^{41–44} To better control the surface composition of the Pd–Cu alloy nanoparticles and to improve selectivity toward the directed hydrogenation, we carried out a variety of

Scheme 2. Changes in Pd–Cu Surface Speciation As a Function of Thermal Treatment Atmosphere, Temperature, and Sequence



thermal annealing steps under both reducing and inert atmospheres.

Mesoporous SiO₂ was chosen as the support for thermal annealing studies due to the superior uniformity and low polydispersity of its supported nanoparticles (Table S13, Figure S27). For the following thermal treatments, we begin with an identical impregnated and calcined material with a 75:25 Pd/Cu ratio on SiO₂. The impregnation is carried out sequentially using metal ammonia precursors, and after calcination, only oxidized Pd and Cu species are observed (Figures S2 and S3). We first performed H₂ reduction on the calcined sample at temperatures ranging from room temperature to 800 °C (Table 1, entries 7–9). At room temperature, only Pd precursors can be reduced by H₂, generating a catalyst comprising reduced Pd nanoparticles interspersed with Cu oxides (RT H₂), which shows identical reactivity and selectivity to pure Pd. Catalyst selectivity increases slightly with increasing reduction temperature due to Pd–Cu alloy formation (600H₂). However, at best, catalysts treated with H₂ alone can achieve modest directivity (3:1 dr) and full conversion over 20 h, consistent with formation of a Pd-rich alloy surface in the high temperature H₂ environment (800H₂).

To generate a more Cu-rich surface, we annealed the calcined sample under N₂ at temperatures between 600 and 800 °C (Table 1, entries 10–12). Due to the lack of an external reductant, higher temperatures are required to reduce the Cu precursors and form the bimetallic alloy using only residual ammonia in the calcined material. At 600 °C under N₂, the catalyst shows high conversion and low directivity due to negligible Cu precursor reduction at this temperature (600N₂). As the N₂ annealing temperature is raised to 700 and 800 °C, the diastereoselectivity rises dramatically to 10:1 and 17:1 dr, respectively, while the conversion drops to 66% and 30% (700N₂, 800N₂).

We then further reduced the catalysts annealed under N₂ at 400 °C in H₂ in order to more efficiently reduce and incorporate the Cu atoms into the alloy nanoparticle (Table 1, entries 13–15). In all cases, the reactivity increases while the diastereoselectivity of the N₂-treated catalyst is retained. Our most selective and active catalyst, 800N₂-400H₂, achieves 16:1 dr and full conversion over 20 h. Raising the reduction temperature up to 800 °C after N₂ annealing (800N₂-800H₂) erodes the dr back down to 6:1 due to segregation of Pd to the surface. On the basis of these data, the optimal catalyst for both high diastereoselectivity and high conversion in this system requires sequential 800N₂-400H₂ treatment in order to obtain a balanced distribution of Pd and Cu on the bimetallic surface.

To understand the structural requirements for efficient substrate-directed hydrogenation, we characterized three $\text{Pd}_3\text{Cu}/\text{SiO}_2$ samples that show distinct selectivity and conversion behavior: 800H_2 , $800\text{N}_2\text{-}400\text{H}_2$, and 800N_2 . All catalysts show similar nanoparticle morphology and Pd–Cu average elemental composition based on scanning-transmission electron microscopy (STEM), energy-dispersive X-ray spectroscopy (EDS), and X-ray fluorescence (XRF; Figures 1 and

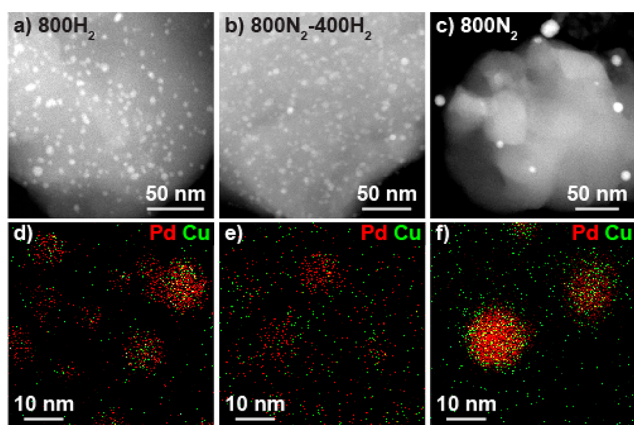


Figure 1. STEM images and EDS maps for $\text{Pd}_3\text{Cu}/\text{SiO}_2$ treated under (a, d) $800\text{ }^\circ\text{C H}_2$, (b, e) $800\text{ }^\circ\text{C N}_2\text{-}400\text{ }^\circ\text{C H}_2$, and (c, f) $800\text{ }^\circ\text{C N}_2$.

S4–S6, Table S1). Powder X-ray diffraction (XRD) shows that all samples possess a face-centered cubic (FCC) crystal structure as expected for a solid-solution Pd–Cu alloy, and all peaks are shifted to a higher 2θ relative to a pure Pd phase (Figure 2a,b). The sample directly reduced in 5% H_2 (800H_2) shows a larger peak shift compared to those annealed first under N_2 . The calculated lattice parameter of 3.833 \AA indicates an approximate $\text{Pd}_{79}\text{Cu}_{21}$ structure for the 800H_2 sample while

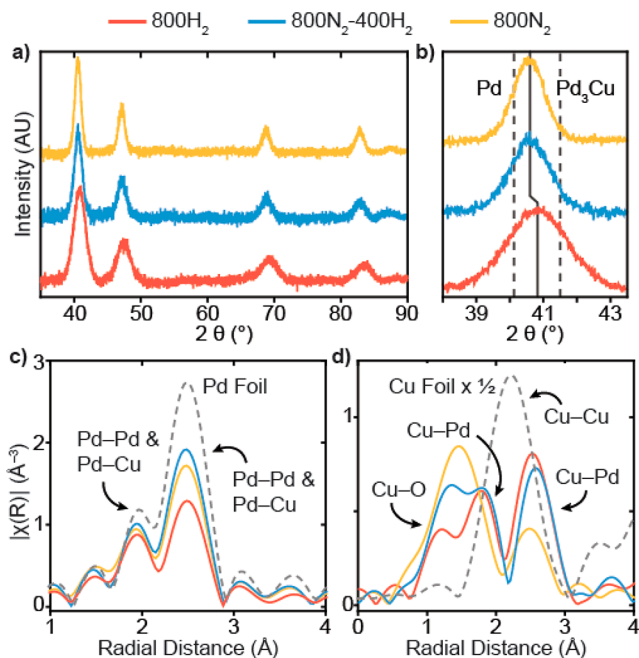


Figure 2. (a) Powder XRD, (b) close-up of XRD (111) peak, (c) Pd K-edge EXAFS, and (d) Cu K-edge EXAFS for $\text{Pd}_3\text{Cu}/\text{SiO}_2$ catalysts.

the 800N_2 and $800\text{N}_2\text{-}400\text{H}_2$ samples have lattice parameters of 3.854 \AA and $\text{Pd}_{87}\text{Cu}_{13}$ composition (Table S2).

X-ray absorption fine structure (EXAFS) at the Pd K-edge shows that all samples possess the characteristic two-peak shape of the FCC crystal structure (Figure 2c). Fitting the EXAFS spectrum allows us to determine the coordination numbers (CN) and bond distances (R) for all atoms within the first coordination sphere (Table 2, Table S3, Figure S8). Consistent with XRD, EXAFS indicates that the largest amount of Pd–Cu alloying is observed in the 800H_2 sample followed by the $800\text{N}_2\text{-}400\text{H}_2$ and 800N_2 samples based on the ratio of Pd–Pd to Pd–Cu CN. The 800N_2 sample also shows residual Pd–O scattering due to incomplete reduction of Pd precursors. At the Cu K-edge, all samples show significant un-reduced Cu–O scattering in addition to Cu–Pd scattering (Figure 2d). The ratio of Cu–Pd to Cu–O CN in each sample parallels the degree of alloying observed at the Pd K-edge and in the XRD pattern (Table 2, Figure S9). On the basis of these data, we conclude that the bulk Pd–Cu alloy structure does not dictate catalyst diastereoselectivity. In fact, the catalyst with the highest degree of bulk alloying, 800H_2 , showed the lowest directed hydrogenation selectivity, corroborating our hypothesis that the surface composition must vary based on the thermal treatment sequence and environment.

The scattering amplitude in the Pd K-edge EXAFS spectrum, which reflects the total first-shell coordination around Pd atoms, provides indirect information about the enrichment of Pd atoms on the surface or in the core of the nanoparticle (Figure 2c, Table 2).^{34,45,46} The low directivity 800H_2 catalyst has the lowest EXAFS scattering intensity and a total Pd–M CN of 8.6, significantly lower than the expected CN of 12 for bulk Pd atoms in an FCC structure and characteristic of Pd enrichment at the surface of the nanoparticle. In contrast, the strongly directing $800\text{N}_2\text{-}400\text{H}_2$ catalyst has a similar average nanoparticle size but shows much higher scattering intensity and a total Pd–M CN of 11.2 (Figure S6). We also characterized another low directivity sample ($800\text{H}_2/\text{Al}_2\text{O}_3$) with larger average particle size compared to the SiO_2 samples (Figure S10). The $800\text{H}_2/\text{Al}_2\text{O}_3$ sample has a total Pd–M CN of 9.4, higher than the total CN on $800\text{H}_2/\text{SiO}_2$ due to the larger particles, but still in a regime that represents significant surface Pd speciation (Table S3). Unfortunately, total coordination number cannot be analyzed when residual oxide remains in the sample, as is the case for the 800N_2 sample and all EXAFS data at the Cu K-edge. In addition, we obtained STEM-EDS mapping and CO chemisorption data on the thermally treated $\text{Pd}_3\text{Cu}/\text{SiO}_2$ samples, but neither measurement has sufficient resolution to clearly distinguish the relative distribution of Pd and Cu atoms on the nanoparticle surface (Figure 1d–f, Table S5). Together with the literature on Pd–Cu surface segregation, these data suggest that subtle changes to bimetallic surface composition engendered by the thermal treatments have a strong impact on directed hydrogenation behavior.

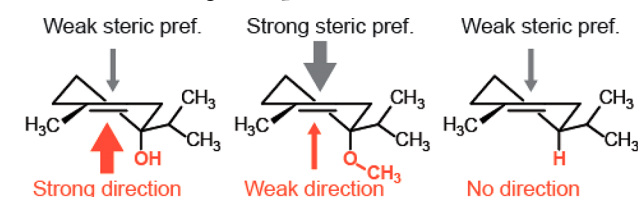
In order to confirm that the diastereoselectivity observed on the Pd–Cu alloy catalysts is in fact due to a hydroxyl directing effect, we prepared two analogues of terpinen-4-ol ($R = \text{OH}$) with different directing groups. Terpinen-4-ol methyl ether ($R = \text{OCH}_3$) should have weaker directing ability because the bulky methyl group decreases the binding affinity of the oxygen atom to the surface while p-menthene ($R = \text{H}$) should exhibit no direction whatsoever (Scheme 3). When two $\text{Pd}_3\text{Cu}/\text{SiO}_2$ catalysts (800H_2 , $800\text{N}_2\text{-}400\text{H}_2$) are compared to pure Pd/

Table 2. Pd and Cu K-edge XAS Fitting Parameters for Thermally Treated Pd₃Cu/SiO₂ Catalysts

sample	edge	scattering pair	CN	R (Å)	σ^2 (Å ²) ^a	E ₀ (eV)
Pd ₃ Cu/SiO ₂ 800 °C H ₂	Pd	Pd–Pd	7.0 ± 0.6	2.717 ± 0.005	0.005	–5.0 ± 0.6
		Pd–Cu	1.6 ± 0.6			
	Cu	Cu–O	1.9 ± 0.4	1.917 ± 0.018	0.009	–3.4 ± 0.7
Pd ₃ Cu/SiO ₂ 800 °C N ₂ + 400 °C H ₂	Pd	Cu–Pd	4.8 ± 0.5	2.680 ± 0.008		
		Pd–Pd	9.8 ± 0.4	2.728 ± 0.002	0.005	–6.3 ± 0.3
	Cu	Pd–Cu	1.4 ± 0.4			
		Cu–O	3.0 ± 0.3	1.924 ± 0.007	0.009	–2.3 ± 0.4
Pd ₃ Cu/SiO ₂ 800 °C N ₂	Pd	Cu–Pd	3.9 ± 0.3	2.725 ± 0.006		
		Pd–O	1.4 ± 0.4	2.041 ± 0.028	0.005	–6.5 ± 0.4
		Pd–Pd	8.3 ± 0.5	2.729 ± 0.003		
	Cu	Pd–Cu	0.8 ± 0.5			
		Cu–O	4.1 ± 0.1	1.928 ± 0.003	0.009	–3.0 ± 0.3
		Cu–Pd	1.8 ± 0.2	2.710 ± 0.007		

^a σ^2 values are determined based on metal foil references and fixed during the EXAFS fitting.

Scheme 3. Steric vs Directing Selectivity Preferences for Different Directing Groups



SiO₂, we indeed observe that the directing effect is attenuated upon methylation or removal of the hydroxyl functional group. The methyl ether substrate has a strong steric selectivity preference due to the bulky methoxy group in the axial position, which is reflected in the 1:7 dr (P1/P2) on pure Pd (Table 3). While there is an increase in dr toward the directed product from 1:7 to 1:4 and 1:2 using Pd–Cu catalysts, the weak direction can never overcome the steric preference. When no directing group is present (R = H), no change in diastereoselectivity is observed between the monometallic Pd and Pd–Cu catalysts. The hydrogenated product exhibits a dr

of ~1:3 on all catalysts due to the inherent steric preference of the substrate, illustrating that the geometric and electronic changes to the catalyst surface that accompany alloy formation do not affect diastereoselectivity in the absence of a directing group. The rates of reaction should also be sensitive to the strength of directing group binding to the surface, which is observed on both Pd–Cu alloy catalysts. The nondirecting R = H substrate shows lower reactivity by a factor of 3 and 6 relative to R = OH and OMe substrates, respectively, because no oxygen functionality is present to facilitate substrate adsorption onto Cu surface atoms.

We also evaluated a few additional substrates to identify the key features that enable highly diastereoselective heterogeneous directed hydrogenation (Table 4). Both homoallylic (entries 1, 2) and allylic alcohols (entries 3–8) are capable of directing the diastereoselective hydrogen addition, provided at least one additional substituent besides the OH group is present on the cyclohexene ring to reduce conformational flexibility. In particular, substrates in which the OH directing group prefers an axial position in the half-chair conformation result in the highest diastereoselectivities (entries 1, 2, 3, 6). Substrates wherein the directing group prefers an equatorial position or has no conformational preference (entries 4, 5, 7, 8) show weaker directing effects but still noticeable increases in diastereomeric ratio relative to the pure Pd/SiO₂ control.

Finally, we performed kinetics and reusability studies on our optimized Pd₃Cu/SiO₂ catalyst to understand surface structural evolution and catalyst stability over time. We first measured conversion and selectivity for terpinen-4-ol hydrogenation over time using a freshly prepared catalyst. Interestingly, the diastereoselectivity of the catalyst increases significantly over the first 6 h of the reaction, likely due to bimetallic surface reconstruction that occurs upon exposure to the reaction medium (Figure 3). The diastereoselectivity at the end of 20 h of reaction reaches the expected 14:1 dr and 90% conversion. To avoid exposing the catalyst to air, we then injected a second aliquot of the substrate directly into the flask. The reaction continues at a slightly slower rate, but the diastereomeric ratio of the new product formed is high from the outset, corroborating the fact that the catalyst surface reaches a stable state after an initial reconstruction. If we instead filter off the Pd₃Cu/SiO₂ powder and dry it in the air, we find that the reactivity of the catalyst drops significantly upon reuse though the diastereoselectivity remains high, indicating that the alloy surface deactivates significantly upon

Table 3. Diastereoselectivity and Conversion for Three Directing Groups over Pd/SiO₂ and Pd₃Cu/SiO₂ Catalysts

catalyst	dr (P1:P2) ^a at high conversion		
	R = OH	R = OMe	R = h
Pd/SiO ₂	1:3	1:7	1:3
Pd ₃ Cu 800H ₂	3:1	1:4	1:3
Pd ₃ Cu 800N ₂ –400H ₂	16:1	1:2	1:3

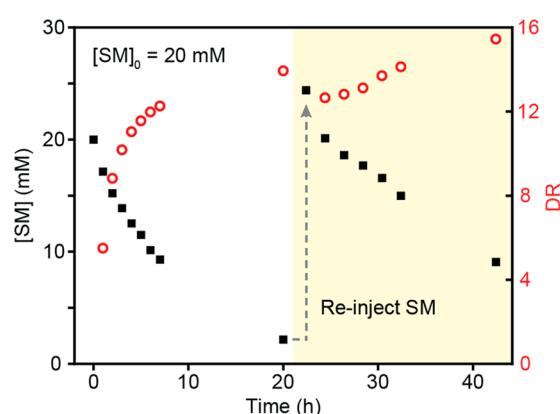
catalyst	conversion (%) at fixed time		
	R = OH	R = OMe	R = H
Pd/SiO ₂ ^b	99	96	74
Pd ₃ Cu 800 H ₂ ^c	31	64	11
Pd ₃ Cu 800N ₂ –400H ₂ ^c	21	49	8

^aDiastereomeric ratios averaged over three runs; standard deviations provided in Table S4. ^bConversions obtained at 2 h. ^cConversions obtained at 4 h.

Table 4. Substrate Scope for Pd₃Cu/SiO₂-Catalyzed Directed Hydrogenation^a

entry	alkene	10 mol% Pd or Pd ₃ Cu/SiO ₂ 1 atm H ₂ , RT, 20 h	%conversion*	DR*	%isomerized*
(1)			Pd: 99% Pd ₃ Cu: 99%	1:3 dr 16:1 dr	<1% <1%
(2)			Pd: 99% Pd ₃ Cu: 71%	1:1 dr 12:1 dr	<1% <1%
(3) [^]			Pd: 99% Pd ₃ Cu: 99%	1:1 dr 24:1 dr	9% 6%
(4) [^]			Pd: 99% Pd ₃ Cu: 99%	2:1 dr 8:1 dr	9% 6%
(5) [^]			Pd: 99% Pd ₃ Cu: 97%	1:2 dr 2:1 dr	6% 5%
(6) [^]			Pd: 99% Pd ₃ Cu: 83%	8:1 dr 22:1 dr	6% 5%
(7)			Pd: 99% Pd ₃ Cu: 99%	1:2 dr 1:1 dr	2% 11%
(8)			Pd: 99% Pd ₃ Cu: 99%	1:1 dr 4:1 dr	<1% 4%

^a(*) Conversion, diastereomeric ratio (dr), and percent isomerization determined by GC with decane as an internal standard except for entry 7, where dr is determined by NMR. (°) Entries 3 and 4 and entries 5 and 6 run as a mixture of diastereomers.

**Figure 3.** Starting material (terpinen-4-ol) concentration and product diastereomeric ratio vs time over a fresh Pd₃Cu/SiO₂ catalyst and after reinjection of a second aliquot of starting material.

oxidation (Table S6). Catalysts that have been exposed to air can be regenerated through a 200 °C H₂ reduction, which then results in 72% conversion and a 12:1 dr over 20 h.

In conclusion, we show that control over the composition of a bimetallic Pd–Cu surface through thermal annealing enables

high diastereoselectivity in the hydroxyl-directed hydrogenation reaction of terpinen-4-ol and related substrates. We postulate that selective binding of the directing group to Cu surface atoms and activation of H₂ and the olefin on neighboring Pd surface atoms enable facially selective hydrogen addition to the olefin with a 16:1 diastereomeric ratio. Future studies will probe the ensemble geometry and adsorption properties of the Pd–Cu surface in greater detail in order to more clearly elucidate the origin of catalyst diastereoselectivity. We anticipate that multimetallic surfaces with well-defined ensemble geometry will enable heterogeneous substrate-directed catalysis that retains the robustness of materials while achieving the stereoselectivity of molecular complexes.

■ ASSOCIATED CONTENT

Supporting Information

The Supporting Information is available free of charge at <https://pubs.acs.org/doi/10.1021/acscatal.1c01434>.

Materials, catalyst synthesis methods, substrate synthesis methods, catalytic hydrogenation methods, physical characterization methods, and supplementary figures and tables (PDF)

■ AUTHOR INFORMATION

Corresponding Author

Christina W. Li – Department of Chemistry, Purdue University, West Lafayette, Indiana 47907, United States; orcid.org/0000-0002-3538-9955; Email: christinawli@purdue.edu

Authors

Alexander J. Shumski – Department of Chemistry, Purdue University, West Lafayette, Indiana 47907, United States
William A. Swann – Department of Chemistry, Purdue University, West Lafayette, Indiana 47907, United States
Nicole J. Escorcía – Department of Chemistry, Purdue University, West Lafayette, Indiana 47907, United States

Complete contact information is available at: <https://pubs.acs.org/doi/10.1021/acscatal.1c01434>

Notes

The authors declare no competing financial interest.

■ ACKNOWLEDGMENTS

This research was supported by Purdue University and the National Science Foundation (CHE-2045013). A.J.S. and C.W.L. acknowledge support from the Purdue Research Foundation. N.J.E. acknowledges support from the NSF under Cooperative Agreement EEC-1647722 and the Engineering Research Center for the Innovative and Strategic Transformation of Alkane Resources (CISTAR). We acknowledge Dr. Joshua Wright, Dr. Mark Warren, Dr. Kamil Kucuk, and Dr. Yujia Ding for assistance with XAS experiments. Use of the Advanced Photon Source is supported by the U.S. Department of Energy, Office of Science, Office of Basic Energy Sciences, under contract DE-AC02-06CH11357. MRCAT operations are supported by the Department of Energy and the MRCAT member institutions.

REFERENCES

- (1) Hoveyda, A. H.; Evans, D. A.; Fu, G. C. Substrate-Directable Chemical Reactions. *Chem. Rev.* **1993**, *93*, 1307–1370.
- (2) Crabtree, R. H.; Felkin, H.; Fillebeenkhan, T.; Morris, G. E. Dihydridoiridium Diolefin Complexes as Intermediates in Homogeneous Hydrogenation. *J. Organomet. Chem.* **1979**, *168*, 183–195.
- (3) Brown, J. M. Directed Homogeneous Hydrogenation. *Angew. Chem., Int. Ed. Engl.* **1987**, *26*, 190–203.
- (4) Stork, G.; Kahne, D. E. Stereocontrol in Homogeneous Catalytic Hydrogenation via Hydroxyl Group Coordination. *J. Am. Chem. Soc.* **1983**, *105*, 1072–1073.
- (5) Crabtree, R. H.; Davis, M. W. Directing Effects in Homogeneous Hydrogenation with $[\text{Ir}(\text{cod})(\text{PCy}_3)(\text{py})]\text{PF}_6$. *J. Org. Chem.* **1986**, *51*, 2655–2661.
- (6) Crabtree, R. H.; Davis, M. W. Occurrence and Origin of a Pronounced Directing Effect of a Hydroxyl Group in Hydrogenation with $[\text{Ir}(\text{cod})\text{P}(\text{C}-\text{Hx}_3(\text{Py}))\text{PF}_6$. *Organometallics* **1983**, *2*, 681–682.
- (7) Evans, D. A.; Morrissey, M. M. Rhodium(I)-Catalyzed Hydrogenation of Olefins. The Documentation of Hydroxyl-Directed Stereochemical Control in Cyclic and Acyclic Systems. *J. Am. Chem. Soc.* **1984**, *106*, 3866–3868.
- (8) Friedfeld, M. R.; Margulieux, G. W.; Schaefer, B. A.; Chirik, P. J. Bis(phosphine)cobalt Dialkyl Complexes for Directed Catalytic Alkene Hydrogenation. *J. Am. Chem. Soc.* **2014**, *136*, 13178–13181.
- (9) Morello, G. R.; Zhong, H. Y.; Chirik, P. J.; Hopmann, K. H. Cobalt-catalyzed alkene hydrogenation: a metallacycle can explain the hydroxyl activating effect and the diastereoselectivity. *Chem. Sci.* **2018**, *9*, 4977–4982.
- (10) Blaser, H. U.; Malan, C.; Pugin, B.; Spindler, F.; Steiner, H.; Studer, M. Selective hydrogenation for fine chemicals: Recent trends and new developments. *Adv. Synth. Catal.* **2003**, *345*, 103–151.
- (11) Augustine, R. L. Selective heterogeneously catalyzed hydrogenations. *Catal. Today* **1997**, *37*, 419–440.
- (12) Heitbaum, M.; Glorius, F.; Escher, I. Asymmetric heterogeneous catalysis. *Angew. Chem., Int. Ed.* **2006**, *45*, 4732–4762.
- (13) Gualandi, A.; Savoia, D. Substrate induced diastereoselective hydrogenation/reduction of arenes and heteroarenes. *RSC Adv.* **2016**, *6*, 18419–18451.
- (14) Huff, B. E.; Khau, V. V.; LeTourneau, M. E.; Martinelli, M. J.; Nayyar, N. K.; Peterson, B. C. Diastereoselectivity in the heterogeneous hydrogenation reactions of phosphorous substituted olefins. *Tetrahedron Lett.* **1997**, *38*, 8627–8630.
- (15) Ranade, V. S.; Consiglio, G.; Prins, R. Functional-group-directed diastereoselective hydrogenation of aromatic compounds. 1. *J. Org. Chem.* **1999**, *64*, 8862–8867.
- (16) Ranade, V. S.; Consiglio, G.; Prins, R. Functional-group-directed diastereoselective hydrogenation of aromatic compounds. 2. *J. Org. Chem.* **2000**, *65*, 1132–1138.
- (17) MaGee, D. I.; Lee, M. L.; Decken, A. Construction of cis- and trans-decahydroisoquinolines via heterogeneous catalytic hydrogenation. *J. Org. Chem.* **1999**, *64*, 2549–2554.
- (18) Borszeki, K.; Mallat, T.; Baiker, A. Diastereoselective hydrogenation at indenols: Evidence for sterically and electronically unfavorable adsorption on palladium. *J. Catal.* **1999**, *188*, 413–416.
- (19) Jiang, C.; Frontier, A. J. Stereoselective synthesis of pyrrolidine derivatives via reduction of substituted pyrroles. *Org. Lett.* **2007**, *9*, 4939–4942.
- (20) Sehgal, R. K.; Koenigsberger, R. U.; Howard, T. J. Effect of Ring Size on Hydrogenation of Cyclic Allylic Alcohols. *J. Org. Chem.* **1975**, *40*, 3073–3078.
- (21) Vile, G.; Albani, D.; Almora-Barrios, N.; Lopez, N.; Perez-Ramirez, J. Advances in the Design of Nanostructured Catalysts for Selective Hydrogenation. *ChemCatChem* **2016**, *8*, 21–33.
- (22) Zhang, L. L.; Zhou, M. X.; Wang, A. Q.; Zhang, T. Selective Hydrogenation over Supported Metal Catalysts: From Nanoparticles to Single Atoms. *Chem. Rev.* **2020**, *120*, 683–733.
- (23) Sankar, M.; Dimitratos, N.; Miedziak, P. J.; Wells, P. P.; Kiely, C. J.; Hutchings, G. J. Designing bimetallic catalysts for a green and sustainable future. *Chem. Soc. Rev.* **2012**, *41*, 8099–8139.
- (24) Edwards, J. K.; Freakley, S. J.; Carley, A. F.; Kiely, C. J.; Hutchings, G. J. Strategies for Designing Supported Gold-Palladium Bimetallic Catalysts for the Direct Synthesis of Hydrogen Peroxide. *Acc. Chem. Res.* **2014**, *47*, 845–854.
- (25) Nguyen, L.; Zhang, S. R.; Wang, L.; Li, Y. Y.; Yoshida, H.; Patlolla, A.; Takeda, S.; Frenkel, A. I.; Tao, F. Reduction of Nitric Oxide with Hydrogen on Catalysts of Singly Dispersed Bimetallic Sites Pt1Com and Pd1Con. *ACS Catal.* **2016**, *6*, 840–850.
- (26) Mori, K.; Sano, T.; Kobayashi, H.; Yamashita, H. Surface Engineering of a Supported PdAg Catalyst for Hydrogenation of CO₂ to Formic Acid: Elucidating the Active Pd Atoms in Alloy Nanoparticles. *J. Am. Chem. Soc.* **2018**, *140*, 8902–8909.
- (27) Boucher, M. B.; Zugic, B.; Cladaras, G.; Kammert, J.; Marcinkowski, M. D.; Lawton, T. J.; Sykes, E. C. H.; Flytzani-Stephanopoulos, M. Single atom alloy surface analogs in Pd_{0.18}Cu_{0.15} nanoparticles for selective hydrogenation reactions. *Phys. Chem. Chem. Phys.* **2013**, *15*, 12187–12196.
- (28) Kyriakou, G.; Boucher, M. B.; Jewell, A. D.; Lewis, E. A.; Lawton, T. J.; Baber, A. E.; Tierney, H. L.; Flytzani-Stephanopoulos, M.; Sykes, E. C. H. Isolated Metal Atom Geometries as a Strategy for Selective Heterogeneous Hydrogenations. *Science* **2012**, *335*, 1209–1212.
- (29) Pei, G. X.; Liu, X. Y.; Yang, X. F.; Zhang, L. L.; Wang, A. Q.; Li, L.; Wang, H.; Wang, X. D.; Zhang, T. Performance of Cu-Alloyed Pd Single-Atom Catalyst for Semihydrogenation of Acetylene under Simulated Front-End Conditions. *ACS Catal.* **2017**, *7*, 1491–1500.
- (30) Armbruster, M.; Kovnir, K.; Behrens, M.; Teschner, D.; Grin, Y.; Schlögl, R. Pd-Ga Intermetallic Compounds as Highly Selective Semihydrogenation Catalysts. *J. Am. Chem. Soc.* **2010**, *132*, 14745–14747.
- (31) Tew, M. W.; Emerich, H.; van Bokhoven, J. A. Formation and Characterization of PdZn Alloy: A Very Selective Catalyst for Alkyne Semihydrogenation. *J. Phys. Chem. C* **2011**, *115*, 8457–8465.
- (32) Pei, G. X.; Liu, X. Y.; Wang, A. Q.; Lee, A. F.; Isaacs, M. A.; Li, L.; Pan, X. L.; Yang, X. F.; Wang, X. D.; Tai, Z. J.; Wilson, K.; Zhang, T. Ag Alloyed Pd Single-Atom Catalysts for Efficient Selective Hydrogenation of Acetylene to Ethylene in Excess Ethylene. *ACS Catal.* **2015**, *5*, 3717–3725.
- (33) Aich, P.; Wei, H. J.; Basan, B.; Kropf, A. J.; Schweitzer, N. M.; Marshall, C. L.; Miller, J. T.; Meyer, R. Single-Atom Alloy Pd-Ag Catalyst for Selective Hydrogenation of Acrolein. *J. Phys. Chem. C* **2015**, *119*, 18140–18148.
- (34) Goulas, K. A.; Sreekumar, S.; Song, Y.; Kharidehal, P.; Gunbas, G.; Dietrich, P. J.; Johnson, G. R.; Wang, Y. C.; Grippo, A. M.; Grabow, L. C.; Gokhale, A. A.; Toste, F. D. Synergistic Effects in Bimetallic Palladium-Copper Catalysts Improve Selectivity in Oxygenate Coupling Reactions. *J. Am. Chem. Soc.* **2016**, *138*, 6805–6812.
- (35) Goulas, K. A.; Song, Y. Y.; Johnson, G. R.; Chen, J. P.; Gokhale, A. A.; Grabow, L. C.; Toste, F. D. Selectivity tuning over monometallic and bimetallic dehydrogenation catalysts: effects of support and particle size. *Catal. Sci. Technol.* **2018**, *8*, 314–327.
- (36) Muslehiddinoglu, J.; Li, J.; Tummala, S.; Deshpande, R. Highly Diastereoselective Hydrogenation of Imines by a Bimetallic Pd-Cu Heterogeneous Catalyst. *Org. Process Res. Dev.* **2010**, *14*, 890–894.
- (37) Furukawa, S.; Suzuki, R.; Komatsu, T. Selective Activation of Alcohols in the Presence of Reactive Amines over Intermetallic PdZn: Efficient Catalysis for Alcohol-Based N-Alkylation of Various Amines. *ACS Catal.* **2016**, *6*, 5946–5953.
- (38) Zafeiratos, S.; Piccinin, S.; Teschner, D. Alloys in catalysis: phase separation and surface segregation phenomena in response to the reactive environment. *Catal. Sci. Technol.* **2012**, *2*, 1787–1801.
- (39) Han, P.; Axnanda, S.; Lyubintsev, I.; Goodman, D. W. Atomic-scale assembly of a heterogeneous catalytic site. *J. Am. Chem. Soc.* **2007**, *129*, 14355–14361.
- (40) Wang, C. Y.; Chen, D. P.; Sang, X. H.; Unocic, R. R.; Skrabalak, S. E. Size-Dependent Disorder-Order Transformation in the Synthesis of Monodisperse Intermetallic PdCu Nanocatalysts. *ACS Nano* **2016**, *10*, 6345–6353.

- (41) Miller, J. B.; Matranga, C.; Gellman, A. J. Surface segregation in a polycrystalline Pd₇₀Cu₃₀ alloy hydrogen purification membrane. *Surf. Sci.* **2008**, *602*, 375–382.
- (42) Zhao, M.; Brouwer, J. C.; Sloof, W. G.; Bottger, A. J. Surface segregation of Pd-Cu alloy in various gas atmospheres. *Int. J. Hydrogen Energy* **2020**, *45*, 21567–21572.
- (43) Bradley, J. S.; Hill, E. W.; Chaudret, B.; Duteil, A. Surface Chemistry on Colloidal Metals. Reversible Adsorbate-Induced Surface Composition Changes in Colloidal Palladium-Copper Alloys. *Langmuir* **1995**, *11*, 693–695.
- (44) Noakes, T. C. Q.; Bailey, P.; Laroze, S.; Bloxham, L. H.; Raval, R.; Baddeley, C. J. Pd/Cu alloys as hydrodechlorination catalysts: a medium-energy ion scattering study of surface composition under exposure to chlorinated hydrocarbons. *Surf. Interface Anal.* **2000**, *30*, 81–84.
- (45) Beale, A. M.; Weckhuysen, B. M. EXAFS as a tool to interrogate the size and shape of mono and bimetallic catalyst nanoparticles. *Phys. Chem. Chem. Phys.* **2010**, *12*, 5562–5574.
- (46) Marinković, N. S.; Sasaki, K.; Adžić, R. R. Nanoparticle size evaluation of catalysts by EXAFS: Advantages and limitations. *Zast. Mater.* **2016**, *57*, 101–109.